Ensemble-Biased Metadynamics: a Molecular Simulation Method to Sample Experimental Distributions

Supporting Information

Fabrizio Marinelli[1*] and José D. Faraldo-Gómez[1*]

[1]Theoretical Molecular Biophysics Section, National Heart, Lung and Blood Institute, National Institutes of Health, Bethesda, Maryland, USA.

*Correspondence: fabrizio.marinelli@nih.gov or jose.faraldo@nih.gov

Appendix 1

We show that Eq. 1 and Eq. 3 (see main text) are equivalent in the limit of infinitesimally small bin intervals. We first assume that the probability distribution of the atomic coordinates $\boldsymbol{X}$ is:

$$\rho(\boldsymbol{X}) = \frac{\exp\{-\beta U(\boldsymbol{X}) + \sum_i \lambda_i h_i[\xi^{\mathrm{f}}(\boldsymbol{X})]\}}{\int d\boldsymbol{X}' \exp\{-\beta U(\boldsymbol{X}') + \sum_i \lambda_i h_i[\xi^{\mathrm{f}}(\boldsymbol{X}')]\}} \quad \text{(Eq. 1)}$$

From this equation, the probability distribution of ξ can be obtained by integrating $\rho(\boldsymbol{X})$ for a fixed value of ξ:

$$\rho'(\xi) = \int d\boldsymbol{X} \rho(\boldsymbol{X}) \delta[\xi - \xi(\boldsymbol{X})] = \frac{\exp\{-\beta F(\xi) + \sum_i \lambda_i h_i(\xi)\}}{\int d\xi' \exp\{-\beta F(\xi') + \sum_i \lambda_i h_i(\xi')\}} \quad \text{(Eq. S1)}$$

By definition, the parameters λ_i in Eq. 1 are those that ensure that $\rho'(\xi) \approx \rho_{\underline{\exp}}(\xi)$; therefore, from Eq. S1 we obtain:

$$\exp\left\{\sum_i \lambda_i h_i(\xi)\right\} = Z \exp\{\ln \rho_{\exp}(\xi) + \beta F(\xi)\} \quad \text{(Eq. S2)}$$

where Z is defined as:

$$Z = \int d\xi' \exp\{-\beta F(\xi') + \sum_i \lambda_i h_i(\xi')\} \quad \text{(Eq. S3)}$$

Taken together, these expressions lead to Eq. 3:

$$\rho(\boldsymbol{X}) = \frac{\exp\{-\beta U(\boldsymbol{X}) + \ln \rho_{\exp}[\xi^{\mathrm{f}}(\boldsymbol{X})] + \beta F[\xi^{\mathrm{f}}(\boldsymbol{X})]\}}{\int d\boldsymbol{X}' \exp\{-\beta U(\boldsymbol{X}') + \ln \rho_{\exp}[\xi^{\mathrm{f}}(\boldsymbol{X}')] + \beta F[\xi^{\mathrm{f}}(\boldsymbol{X}')]\}} \quad \text{(Eq. 3)}$$

Appendix 2

We show that if both w/τ and σ are sufficiently small, the biasing potential constructed in the EBMetaD simulation fulfills Eq. 5, that is:

$$\dot{V}(\xi,t>t_e)\approx\frac{C}{\rho_{\exp}(\xi)}\frac{\exp\{-\beta[F(\xi)+V(\xi,t)]\}}{\int d\xi'\exp\{-\beta[F(\xi')+V(\xi',t)]\}}\approx C \quad \text{(Eq. 5)}$$

Let us assume that $N(t,\ \Delta t)$ is the total number of Gaussians added from time t to $t+\Delta t$, and that $n(\xi,\ t,\ \Delta t)d\xi$ is the number of Gaussians specifically added in the interval $d\xi$ around ξ in the same time-window. The distribution of ξ in this time-window can be written as:

$$\rho_{\text{EBMetaD}}(\xi,t,\Delta t)=n(\xi,t,\Delta t)/N(t,\Delta t) \quad \text{(Eq. S4)}$$

Based on this equation, the change in the EBMetaD biasing potential from time t to $t+\Delta t$ is:

$$V(\xi,t+\Delta t)-V(\xi,t)=\frac{w}{\exp\{S_\rho\}}\int d\xi'\frac{n(\xi',t,\Delta t)}{\rho_{\exp}(\xi')}\exp\left\{-[\xi-\xi']^2/2\sigma^2\right\} \quad \text{(Eq. S5)}$$

If σ is small enough, the Gaussians approximate Dirac delta functions and Eq. S5 can be written as:

$$V(\xi,t+\Delta t)-V(\xi,t)\approx\frac{w\sqrt{2\pi\sigma^2}}{\exp\{S_\rho\}}\frac{n(\xi,t,\Delta t)}{\rho_{\exp}(\xi)}=\frac{wN(t,\Delta t)\sqrt{2\pi\sigma^2}}{\exp\{S_\rho\}}\frac{\rho_{\text{EBMetaD}}(\xi,t,\Delta t)}{\rho_{\exp}(\xi)} \quad \text{(Eq. S6)}$$

We now make the additional assumption that if w/τ is sufficiently small, the shape of the bias potential does not change significantly after a certain equilibration time t_e, and therefore:

$$\rho_{\text{EBMetaD}}(\xi,t>t_e,\Delta t)\propto\exp\{-\beta[F(\xi)+V(\xi,t)\} \quad \text{(Eq. S7)}$$

Under this hypothesis, if we divide Eq. S6 by Δt we obtain an expression analogous to Eq. 5:

$$\dot{V}(\xi,t>t_e)\approx\frac{w\sqrt{2\pi\sigma^2}}{\tau\exp\{S_\rho\}\rho_{\exp}(\xi)}\frac{\exp\{-\beta[F(\xi)+V(\xi,t)]\}}{\int d\xi'\exp\{-\beta[F(\xi')+V(\xi',t)]\}}\approx\frac{w\sqrt{2\pi\sigma^2}}{\tau\exp\{S_\rho\}} \quad \text{(Eq. S8)}$$

The condition that w/τ is small implies that the EBMetaD simulation remains close to equilibrium. Similarly to Metadynamics, this condition can be explicitly imposed by gradually reducing w/τ throughout the simulation (1-3). In practice, EBMetaD converges reasonably well as long as w/τ is such that significant variations in the shape of the biasing potential acting on ξ (say, of a few k_BT) are slower than the equilibration time of any degree of freedom orthogonal to ξ(4-6). An indication of convergence after the initial equilibration stage is an even growth of the biasing potential along ξ (Eq. S8). This equilibration time could be accelerated as in other Metadynamics variants (4), for example using a bias-exchange multi-replica scheme (7). In complex systems it is conceivable that the sampling of the observables for which an experimental distribution is known is hampered by other slow degrees of freedom in the system. In Bias-Exchange Metadynamics (7), independent simulations that apply a bias to different reaction coordinates can be coupled by Metropolis Monte-Carlo exchanges, as in Hamiltonian replica-exchange. In problematic cases, therefore, a

conventional Metadynamics bias could be used in a subset of replicas in order to enhance the reversible exploration of those slow degrees of freedom, while a different replica (or replicas) would utilize the EBMetaD method to reproduce a specific probability distribution.

If the biased variables include the slow degrees of freedom, EBMetaD displays similar features of standard Metadynamics (4-6); that is, the biased probability distribution converges to the experimental histogram as the average biasing potential converges to Eq. 6, for a wide range of possible simulation parameters (see Fig. S1). The instantaneous biasing potential, however, will fluctuate around the average, again as in conventional Metadynamics, to a degree that depends on the parameters defining the biasing potential. This fluctuation range can be described with good accuracy by the following expression (8):

$$\bar{\varepsilon} = \int d\xi\, \varepsilon(\xi,t)\rho_{\exp}(\xi) = C\sqrt{\frac{w\tau_S\sigma}{\tau\beta\exp\{S_\rho\}}} \quad \text{(Eq. S9)}$$

where $\varepsilon(\xi,t)$ is the instantaneous error in the bias potential, defined as:

$$\varepsilon(\xi,t) = \sqrt{\left\langle \left[V(\xi,t) - \left\langle V(\xi,t)\right\rangle\right]^2 \right\rangle} \quad \text{(Eq. S10)}$$

In Eq. S9, τ_S is a relaxation time that depends on the target distribution. For unimodal distributions, $\tau_S \sim [\exp\{S\rho\}]^2/D$, where D is the diffusion coefficient of observable ξ. However, multiple peaks in the target distribution (i.e. free-energy barriers imposed by the bias) imply a larger value of τ_S. For the model systems investigated in this study and the range of parameters explored (Figs. S1), Eq. S9 is fulfilled with $C \sim 0.7$ (Fig. S1E). Eq. S9 can be used to initially select the simulation parameters as in standard Metadynamics, i.e. σ can be selected to match the desired spatial resolution, and w/τ can be tuned so that the average error is in the order of $k_B T$.

Appendix 3

The maximum entropy principle can be easily generalized to multiple observables ξ_j and probability distributions $\rho_{\exp}(\xi_j)$ as a sum the linear perturbations induced separately by each histogram:

$$\rho(\boldsymbol{X}) = \frac{\exp\{-\beta U(\boldsymbol{X}) + \sum_{ij}\lambda_{ij}h_{ij}[\xi_j^{\mathrm{f}}(\boldsymbol{X})]\}}{\int d\boldsymbol{X}'\exp\{-\beta U(\boldsymbol{X}') + \sum_{ij}\lambda_{ij}h_{ij}[\xi_j^{\mathrm{f}}(\boldsymbol{X}')]\}} \quad \text{(Eq. S11)}$$

Similarly to the one-dimensional case, $h_{ij}[\xi_j^{\mathrm{f}}(\boldsymbol{X})] = 1$ if $\xi_j^{\mathrm{f}}(\boldsymbol{X})$ is in bin i and 0 otherwise, and the λ_{ij} parameters ensure that the time averages of $h_{ij}[\xi_j^{\mathrm{f}}(\boldsymbol{X})]$ are equal to the experimental probability values. Also in this case, Eq. S11 can be written in terms of free energies and target probability distributions. Selecting the observable ξ_k and integrating Eq. S11 for a fixed value of ξ_k we obtain:

$$\rho'(\xi_k) = \int d\boldsymbol{X}\rho(\boldsymbol{X})\delta(\xi_k - \xi_k^{\mathrm{f}}(\boldsymbol{X})) = \frac{\exp\{-\beta F_{\mathrm{e}}(\xi_k) + \sum_i \lambda_{ik}h_{ik}\xi_k\}}{\int d\xi_k'\exp\{-\beta F_{\mathrm{e}}(\xi_k') + \sum_i \lambda_{ik}h_{ik}\xi_k'\}} \quad \text{(Eq. S12)}$$

where $F_e(\xi_k)$ is the free energy along ξ_k after the ensemble has been corrected along the other observables $\xi_{j\neq k}$:

$$F_e(\xi_k) = -\frac{1}{\beta}\ln\int d\boldsymbol{X}\,\delta(\xi_k - \xi_k^f(\boldsymbol{X}))\,\exp\{-\beta U(\boldsymbol{X}) + \sum_{i,j\neq k}\lambda_{ij}h_{ij}[\xi_j^f(\boldsymbol{X})]\} \quad \text{(Eq. S13)}$$

As mentioned, the parameters λ_{ij} in Eq. S11 are by definition those that ensure $\rho'(\xi_k) = \rho_{exp}(\xi_k)$; therefore we obtain:

$$\rho(\boldsymbol{X}) = \frac{\exp\{-\beta U(\boldsymbol{X}) + \sum_j \ln(\rho_{exp}[\xi_j^f(\boldsymbol{X})]) + \sum_j \beta F_e[\xi_j^f(\boldsymbol{X})]\}}{\int d\boldsymbol{X}'\exp\{-\beta U(\boldsymbol{X}') + \sum_j \ln(\rho_{exp}[\xi_j^f(\boldsymbol{X}')]) + \sum_j \beta F_e[\xi_j^f(\boldsymbol{X}')]\}} \quad \text{(Eq. S14)}$$

Analogously the free energies $F_e(\xi_k)$ can be defined as:

$$F_e(\xi_k) = -\frac{1}{\beta}\ln\int d\boldsymbol{X}\,\delta(\xi_k - \xi_k^f(\boldsymbol{X}))\,\exp\{-\beta U(\boldsymbol{X}) + \sum_{j\neq k}\ln(\rho_{exp}[\xi_j^f(\boldsymbol{X})]) + \sum_{j\neq k}\beta F_e[\xi_j^f(\boldsymbol{X})]\} \quad \text{(Eq. S15)}$$

In practice, in EBMetaD the multi-dimensional ensemble correction is provided by a sum of biasing potentials for each observable:

$$V(\xi_1,\xi_2,\ldots,t) = \sum_j V(\xi_j,t) = \sum_j \sum_{t'=\tau,2\tau\ldots}^{t} \frac{w_j \exp\left\{-[\xi_j - \xi_j^f(\boldsymbol{X}_{t'})]^2 / 2\sigma_j^2\right\}}{\exp\{S_{\rho_j}\}\rho_{exp}[\xi_j^f(\boldsymbol{X}_{t'})]} \quad \text{(Eq. S16)}$$

That is, several one-dimensional biasing potentials are constructed concurrently, rather than a single multi-dimensional potential (as in standard Metadynamics), which results in faster convergence (9). Similarly to the one dimensional case, if w_j/τ is sufficiently small, for $t > t_e$ the simulation reaches a stationary condition in which the instantaneous biasing potential oscillates around the theoretical profile expected from the maximum-entropy principle (Eq. S14), and thus the distribution along each observable matches the target probability density, that is:

$$\bar{V}(\xi_j, t > t_e) \approx -\frac{1}{\beta}\ln(\rho_{exp}[\xi_j^f(\boldsymbol{X})]) - F_e[\xi_j^f(\boldsymbol{X})] \quad \text{(Eq. S17)}$$

Supplementary Methods

Langevin Dynamics simulations – The functional form of the potential in Fig. 1A and Fig. S2A is:

$$
\begin{aligned}
U(\xi,\xi') = \; & -11.4\times\exp\left\{-\frac{1}{2}\left[\frac{\xi+\xi'}{\sqrt{2}}\right]^2\right\}\exp\left\{-\frac{1}{2\times1.5^2}\left[\frac{\xi-\xi'}{\sqrt{2}}\right]^2\right\} \\
& -11.4\times\exp\left\{-\frac{1}{2\times1.5^2}\left[\frac{\xi+\xi'}{\sqrt{2}}-3.5\right]^2\right\}\exp\left\{-\frac{1}{2\times1.5^2}\left[\frac{\xi-\xi'}{\sqrt{2}}\right]^2\right\} \\
& -10.2\times\exp\left\{-\frac{1}{2\times1.5^2}\left[\frac{\xi+\xi'}{\sqrt{2}}\right]^2\right\}\exp\left\{-\frac{1}{2}\left[\frac{\xi-\xi'}{\sqrt{2}}-4.3\right]^2\right\} \\
& -10.2\times\exp\left\{-\frac{1}{2\times1.5^2}\left[\frac{\xi+\xi'}{\sqrt{2}}\right]^2\right\}\exp\left\{-\frac{1}{2}\left[\frac{\xi-\xi'}{\sqrt{2}}+4.3\right]^2\right\} \\
& -11.4\times\exp\left\{-\frac{1}{2\times1.5^2}\left[\frac{\xi+\xi'}{\sqrt{2}}+3.5\right]^2\right\}\exp\left\{-\frac{1}{2\times1.5^2}\left[\frac{\xi-\xi'}{\sqrt{2}}\right]^2\right\}
\end{aligned}
$$

Molecular Dynamics simulations – The simulations of T4 lysozyme were carried out with NAMD 2.9 (10) and a modified version of PLUMED (9) that implements EBMetaD. We used the CHARMM27/CMAP (11,12) forcefield for the protein and solvent, and the parameters of Sezer et al. (13) for the spin-labels. The simulations were carried out at constant temperature (298 K) and pressure (1 atm) using periodic boundary conditions in all directions, and a time-step of 2 fs. Electrostatic interactions were calculated using Particle-Mesh-Ewald with a real-space cut-off of 12 Å; the same cut-off distance was used for van der Waals interactions. The variables considered in the EBMetaD simulations were the pairwise distances between the centers of mass of the nitroxide groups in the spin-labels. Gaussians of height 0.05 kcal/mol and width 0.5 Å were added every 2 ps (i.e. every 10^3 steps), and scaled by the experimental probability distributions according to Eq. 7 (see main text). This height was selected on the basis of Eq. S9, so that the average error of the average biasing potential is in the order of k_BT. To evaluate Eq. S9, we considered $\tau_S \sim [\exp\{S\rho\}]^2/D$ and $D \sim 0.1$ Å^2/ps was estimated from the standard MD simulation as the initial slope of the mean-square displacement of the spin-label distances (e.g. $D \sim 0.05$ Å^2/ps for the 62-134 pair). The standard deviation of the biasing potential around the average, calculated *a posteriori* via Eq. S10 is in good agreement with the initial estimate (based on Eq. S9), namely 1.5 k_BT, 2 k_BT and k_BT for spin-label pairs 62-109, 62-134 and 109-134, respectively.

Supplementary Figures

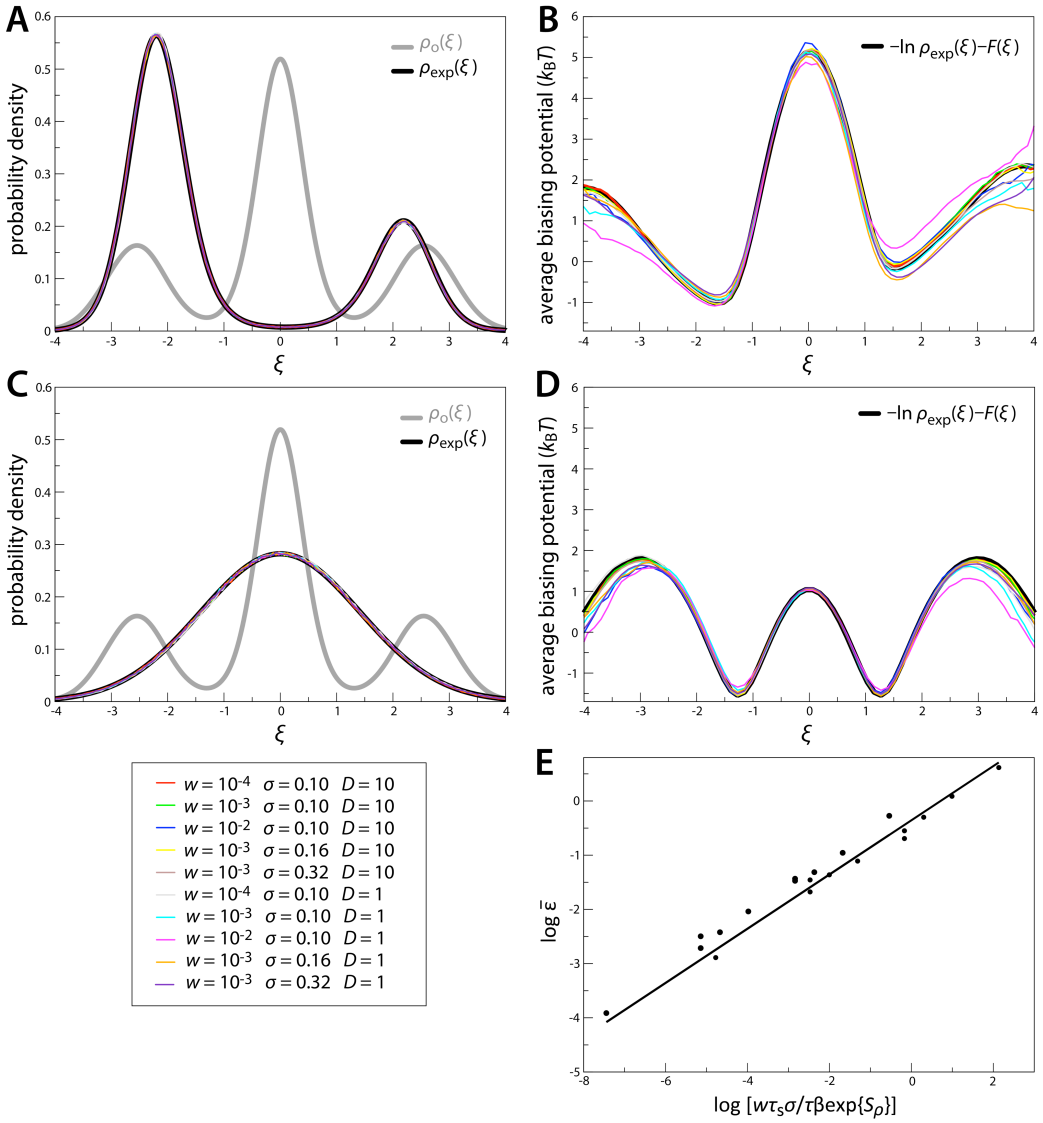

Figure S1. Robustness of the EBMetaD method against variations in the parameters defining the biasing potential (Eq. 4), for the model 2D potential shown in Fig. 1. **(A)** Bi-modal target probability distributions $\rho_{exp}(\xi)$ (black) compared with the distributions obtained with EBMetaD simulations (colored lines), for different values of the nominal height and width of the biasing Gaussians, w and σ, respectively, and for different values of the diffusion constant, D. (**B**) The average biasing potential resulting from the EBMetaD simulations (colored lines) is compared with the theoretical results, calculated analytically (see caption of Fig. 1). (**C**, **D**) Same as (A, B), for a unimodal target probability distribution. (**E**) Error in the average biasing potential as a function of the EBMetaD simulation parameters demonstrates validity of Eq. S9. For the target distribution shown in panel (B), we used $\tau_S \sim [\exp\{S\rho\}]^2/D$, while for that in panel (A), τ_S was scaled by an Arrhenius factor on account of the free energy barrier, i.e. $\tau_S \sim 20\ [\exp\{S\rho\}]^2/D$. The data fulfills the linear relationship in Eq. S9 with $C \sim 0.7$.

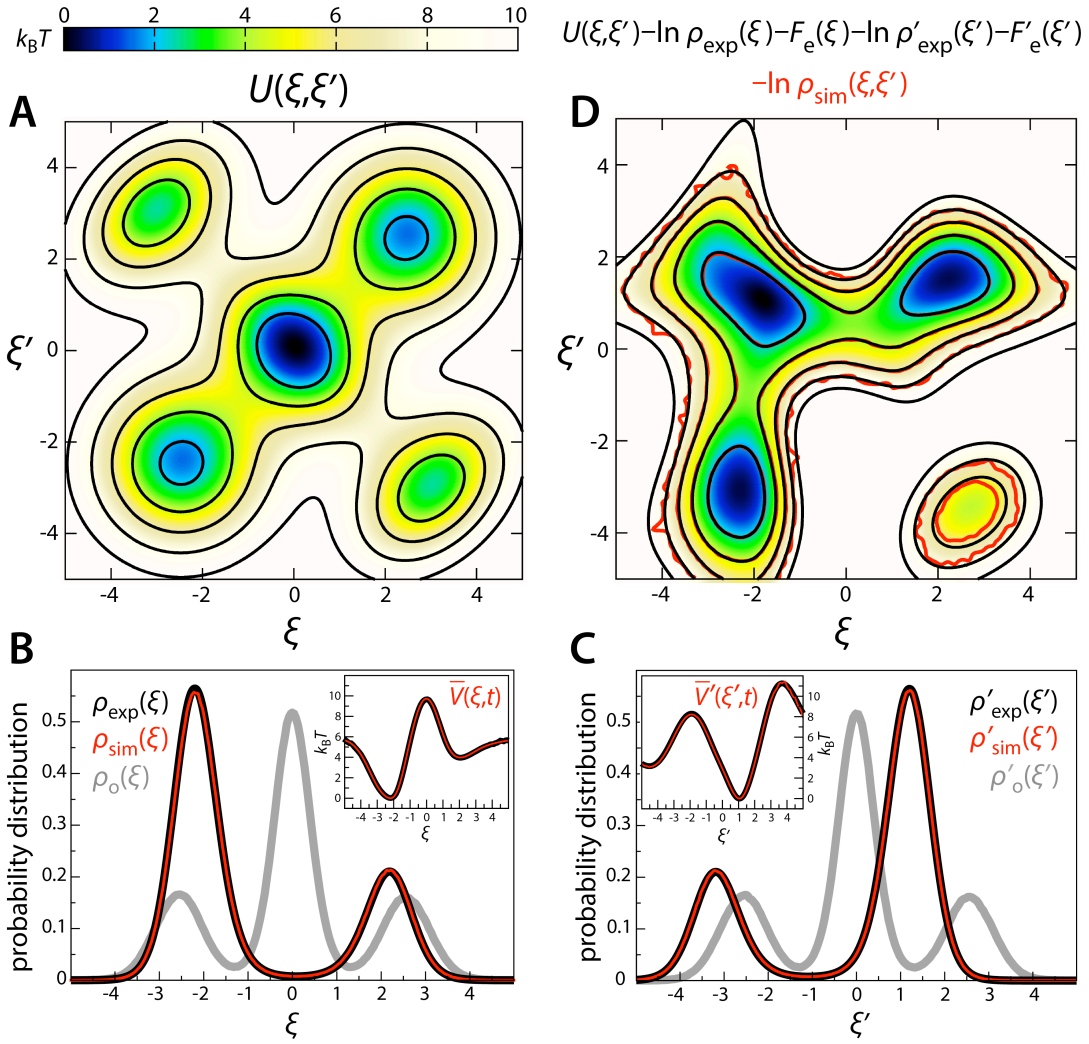

Figure S2. (**A**) Model 2D potential used to test EBMetaD, via an overdamped Langevin dynamics simulation. (**B, C**) Histograms of ξ and ξ' calculated directly from the EBMetaD simulation (red lines), compared with the probability distributions associated with the model potential (gray), and with the target distributions (black). *Insets*: average biasing potentials in each case, compared with $-ln\ \rho_{exp}(\xi)\ -F_e(\xi)$ and $-ln\ \rho'_{exp}(\xi')\ -F'_e(\xi')$ (see Eq. S18), with $t_e = 5\times10^5$ steps. $F_e(\xi)$ and $F'_e(\xi')$ were calculated analytically (see Appendix 3). (**D**) Histogram of ξ and ξ' from the EBMetaD simulation (red isolines), overlaid on the ensemble-corrected potential calculated analytically (black isolines) (see Appendix 3). Diffusion coefficients in ξ and ξ' were set to 10, the integration time step was 10^{-5} and $k_BT = 1$. Gaussians of height 10^{-4} k_BT and width 0.1 were added to the biasing potential every 10^3 steps.

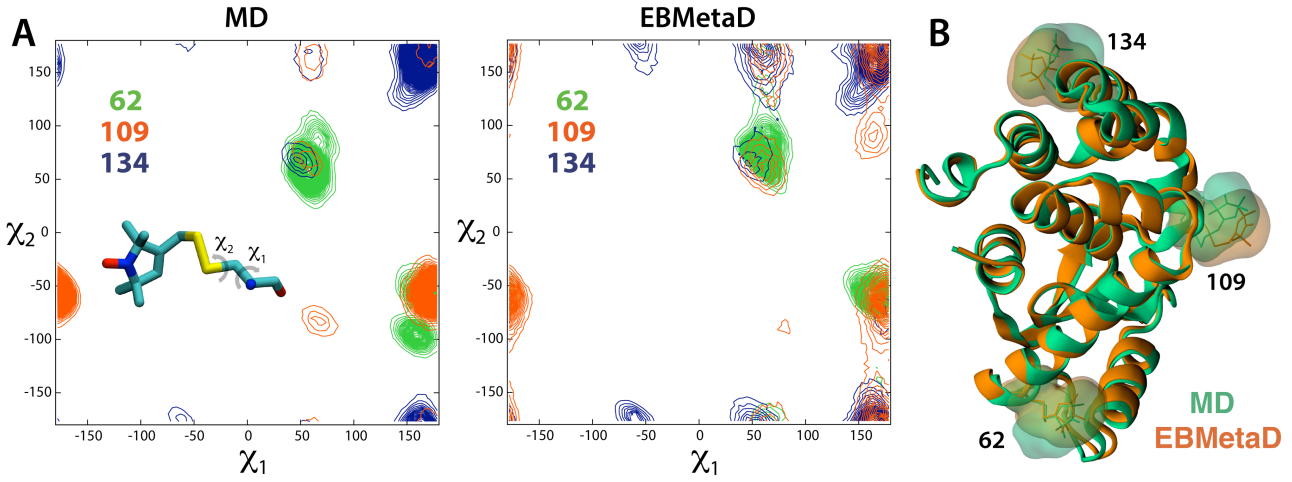

Figure S3. Rotameric configurations of the spin-labels explored in the EBMetaD and unbiased MD simulations of T4 lysozyme. (**A**) Contoured histograms of the χ_1 and χ_2 dihedral angles for each of three spin-labels (structure shown as inset). (**B**) Time-averaged backbone structure in the MD and EBMetaD trajectories, along with volume occupancy maps for each of the spin-labels.

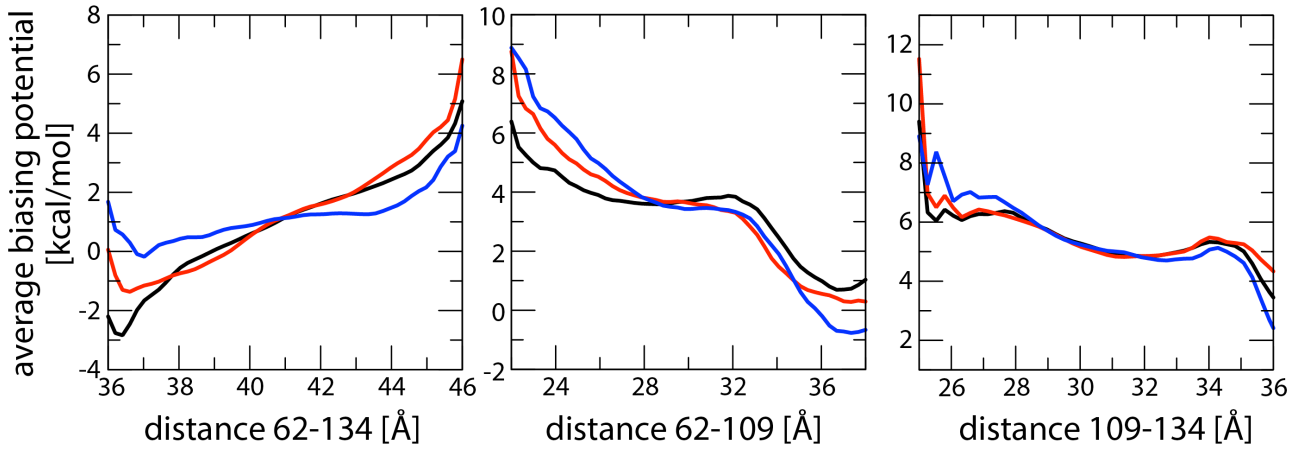

Figure S4. Time-averaged biasing potentials for each of the three spin-label distances targeted in the EBMetaD simulations of T4 lysozyme, for three time-windows of simulation of approximately 65 ns each. If we denote these average potentials as V_1 (black), V_2 (blue), and V_3 (red), the average biasing potentials shown in the insets of Fig. 2B are $V_o = \Sigma\ V_i / N$ (N = 3), for each of the distances, while the corresponding error bars are equal to $[\Sigma\ (V_i - V_o)^2 / N\ (N\text{-}1)]^{1/2}$. Note that in order to calculate these error bars, the biasing potentials accumulated at different time-points, these potentials need to be shifted, as in the figure. Here, the instantaneous biasing potentials $V(\xi,t)$ are shifted by an offset $V_{ref}(t) = \int d\xi\ V(\xi,t)\ \rho_{exp}(\xi)$, where $\rho_{exp}(\xi)$ is the target probability distribution. The standard deviation around the average biasing potential, calculated *a posteriori* (via Eq. S10) is in good agreement with the initial theoretical estimate in Eq. S9, namely 1.5 k_BT, 2 k_BT and k_BT for spin labels 62-109, 62-134 and 109-134, respectively.

Supplementary References

1. Dama, J. F., M. Parrinello, and G. A. Voth. 2014. Well-tempered Metadynamics converges asymptotically. Phys. Rev. Lett. 112:240602.
2. Dama, J. F., G. Rotskoff, M. Parrinello, and G. A. Voth. 2014. Transition-tempered metadynamics: robust, convergent Metadynamics via on-the-fly transition barrier estimation. J. Chem. Theor. Comp. 10:3626-3633.
3. Barducci, A., G. Bussi, and M. Parrinello. 2008. Well-tempered metadynamics: a smoothly converging and tunable free-energy method. Phys. Rev. Lett. 100:020603.
4. Laio, A. and F. L. Gervasio. 2008. Metadynamics: a method to simulate rare events and reconstruct the free energy in biophysics, chemistry and material science. Rep. Prog. Phys. 71:126601.
5. Crespo, Y., F. Marinelli, F. Pietrucci, and A. Laio. 2010. Metadynamics convergence law in a multidimensional system. Phys. Rev. E 81:055701.
6. Bussi, G., A. Laio, and M. Parrinello. 2006. Equilibrium free energies from nonequilibrium metadynamics. Phys. Rev. Lett. 96:090601.
7. Piana, S. and A. Laio. 2007. A bias-exchange approach to protein folding. J. Phys. Chem. B 111:4553-4559.
8. Laio, A., A. Rodriguez-Fortea, F. L. Gervasio, M. Ceccarelli, and M. Parrinello. 2005. Assessing the accuracy of metadynamics. J. Phys. Chem. B 109:6714-6721.
9. Gil-Ley, A. and G. Bussi. 2015. Enhanced conformational sampling using replica exchange with collective-variable tempering. J. Chem. Theor. Comp. 11:1077-1085.
10. Phillips, J. C., R. Braun, W. Wang, J. Gumbart, E. Tajkhorshid, E. Villa, … K. Schulten. 2005. Scalable molecular dynamics with NAMD. J. Comp. Chem. 26:1781-1802.
11. MacKerell, A. D., D. Bashford, M. Bellott, R. L. Dunbrack, J. D. Evanseck, M. J. Field, … M. Karplus. 1998. All-atom empirical potential for molecular modeling and dynamics studies of proteins. J. Phys. Chem. B 102:3586-3616.
12. Mackerell, A. D., M. Feig, and C. L. Brooks. 2004. Extending the treatment of backbone energetics in protein force fields: Limitations of gas-phase quantum mechanics in reproducing protein conformational distributions in molecular dynamics simulations. J. Comp. Chem 25:1400-1415.
13. Sezer, D., J. H. Freed, and B. Roux. 2008. Parametrization, molecular dynamics simulation, and calculation of electron spin resonance spectra of a nitroxide spin label on a polyalanine alpha-helix. J. Phys. Chem. B 112:5755-5767.